Journal of Mechanical Science and Technology (KSME Int. J.), Vol. 19, No. 7, pp. 1449~1459, 2005 1449

Local Flow Speed Measurement Using Tunable AC Thermal Anemometry

Won Seok Chung
Micro Thermal System Research Center, Seoul National University, Seoul 151-742, Korea
Ohmyoung Kwon*
Department of Mechanical Engineering, Korea University, Seoul 136-701, Korea
Joon Sik Lee
School of Mechanical and Aerospace Engineering, Seoul National University, Seoul 151-742, Korea
Young Ki Choi
School of Mechanical Engineering, Chung-Ang University, Seoul 156-756, Korea
Seungho Park
Department of Mechanical and System Design Engineering, Hongik University, Seoul 121-791, Korea

This paper shows the results of local flow speed measurement using tunable AC thermal anemometry, which is suitable for the accurate measurement of wide range flow speed. The measurement accuracy is verified through the comparison between the measurement data and the analytic solution of the sensor temperature oscillation in stationary fluid. The relation between the phase lag and the flow speed is experimentally investigated at various conditions. The measurement sensitivity for low flow speed improves in a low frequency region and that for high flow speed improves in a high frequency region. Also, the sensitivity increases with decreasing thermal conductivity of the surrounding fluid. The local flow speed could be measured as low as 1.5 mm/s and the highest measurement resolution was 0.05 mm/s in the range of 4.5~5.0 mm/s at 1 Hz in this experiment.

Key Words : Flow Speed Measurement, Steady Periodic Heat Transfer, 3ω Voltage, Phase Lag

Nomenclature

b : Width of channel [m]
C_1, C_2 : Constant of integration
c : Height of channel [m]
c_p : Specific heat [J/kg·K]
d_p : Complex quantity defined as $\sqrt{\alpha/i2\omega}$
f : Frequency [Hz]
h : Heat transfer coefficient [W/m²·K]
I : Electric current [A]
I_n : Modified Bessel function of the first kind of order n
i : Imaginary unit, $\sqrt{-1}$
K_n : Modified Bessel function of the second kind of order n
k : Thermal conductivity [W/m·K]
p : Pressure [N/m²]
Q : Flow rate [m³/s]
$\dot{q}$: Heat generation per unit volume [W/m³]
R : Electric resistance [Ω]

* *Corresponding Author,*
E-mail : omkwon@korea.ac.kr
TEL : +82-2-3290-3371; **FAX** : +82-2-926-9290
Department of Mechanical Engineering, Korea University, Seoul 136-701, Korea. (Manuscript **Received** January 12, 2005; **Revised** May 31, 2005)

r : Radius [m] ; radial coordinates
T : Temperature [K]
t : Time [s]
u : Flow speed [m/s]
$V_{3\omega}$: Electric voltage at frequency of 3ω [V]
x, y, z : Coordinates in Cartesian system

Greek symbols

α : Thermal diffusivity [m^2/s] ; temperature coefficient of resistance [1/K]
θ : Complex temperature which represents both amplitude and phase lag [K]
μ : Viscosity [$N \cdot s/m^2$]
ρ : Density [kg/m^3]
ϕ : Phase lag [°]
ω : Angular frequency [rad/s]

Superscripts

$*$: Non-dimensional form

Subscripts

0 : Amplitude of oscillation
f : Fluid
s : Sensor

1. Introduction

With the rapid development of micromachining technology, microfluidic devices are widely used in various applications, such as in separation and analysis of chemicals or in drug delivery, in recent years. The accurate measurement of the low speed flow is indispensable in order to control these microfluidic systems precisely. Although numerous micro flow sensors, which are based on various working principles (Czaplewski et al., 2004 ; Ernst et al., 2002 ; Oosterbroek et al., 1999 ; Wu et al., 2001 ; Wu and Sansen, 2002), have been developed, an adequate sensor with a simple structure that can cover a wide flow speed range with high accuracy is still difficult to find. To address this issue we suggested a novel flow measurement technique, 'tunable AC thermal anemometry' that allows simple integration, robust measurement, and extremely high accuracy in previous research (Chung et al., 2004).

Figure 1 shows the working principle of the tunable AC thermal anemometry. When there is periodic heat generation at frequency of 2ω inside

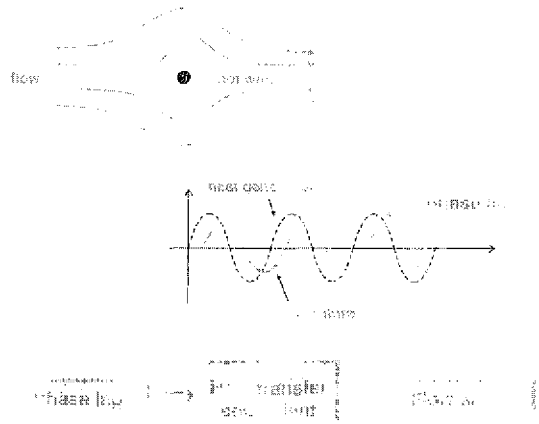

Fig. 1 Principle of AC type thermal anemometry

the cylinder located in a flow field, the temperature of the cylinder oscillates at the same frequency of 2ω with a phase lag relative to the heat generation. From a first order system analysis, the amplitude $T_{s,0}$ and the phase lag ϕ of the cylinder temperature oscillation are given as (Chung et al., 2004)

$$T_{s,0}=\frac{r_s \dot{q}_0}{2\sqrt{h^2+(\rho_s c_{p,s} r_s \omega)^2}} \tag{1}$$

$$\phi=\tan^{-1}\left(-\frac{\rho_s c_{p,s} r_s \omega}{h}\right) \tag{2}$$

where r_s is the radius of the cylinder, $\dot{q}_0$ is the amplitude of the heat generation per unit volume, ρ_s and $c_{p,s}$ are the density and the specific heat of the cylinder, and h is the heat transfer coefficient. Since the phase lag is a sensitive function of the heat transfer coefficient, which is closely related to flow speed, one can measure flow speed by measuring the phase lag.

Tunable AC thermal anemometry has several advantages inherent to its principle over the conventional thermal anemometry. First, since this technique measures only the phase lag at the heating frequency, this is not susceptible to environmental temperature variations. Second, fluid heating can be minimized, because the heater and the sensor are identical and the phase lag is independent of heating power in principle. Third, thanks to the well-developed modern digital signal processing technology, the phase lag can be measured with extreme accuracy, which translates

into the exceptional flow speed measurement accuracy. Fourth, the technique can measure a wide range of flow speed by adjusting the heating frequency. We named this new AC type flow measurement technique 'tunable' AC thermal anemometry, because one can obtain maximum measurement sensitivity by 'tuning' the measurement frequency to flow speed range measured. Lastly, its simple structure makes it suitable for microfabrication process. Therefore, tunable AC thermal anemometry is appropriate for wide range of applications and especially suitable for the accurate flow speed measurement in microfluidic system.

However, one should understand that h in Eq. (2) is not the usual heat transfer coefficient defined at a constant temperature or heat flux condition. We could not find any data for the heat transfer coefficient defined in the steady periodic state in the open literatures. The goal of this study is to obtain the relation between the phase lag and the flow speed as exactly as possible so that tunable AC thermal anemometry can be used as an effective flow speed measurement tool.

This paper is organized as follows. In section 2, experimental apparatus is designed to measure a fully developed laminar flow in a channel with a rectangular cross section. In section 3, the amplitude and the phase lag of the sensor temperature oscillation in the fluid at rest are measured and compared with the analytic solution of the sensor temperature oscillation in order to verify the measurement accuracy. In section 4, a set of experiments is conducted as the material of the sensor and the fluid and the angle between the sensor and the flow are all varied to obtain the relations between the phase lag and the flow speed. Finally, performance tests for the AC type thermal anemometry are carried out to find the lowest measurable flow speed and the highest resolution in this experimental setup.

2. Experimental Details

The schematic of the experimental setup is shown in Fig. 2. Two kinds of metal wires were selected as a sensor : a tungsten wire and a compound metal wire of platinum and rhodium (PtRh). The length of the wires was 1 mm and diameter was 5 μm. These wires were inserted into the channel with a rectangular cross section. The channel was designed to form a fully developed laminar flow and to measure the local flow speed at various vertical positions of the wire and also various angles between the wire and the flow. The width of the channel was 40 mm and height was 4 mm. A vernier caliper is used for changing the vertical position of the wire and it has the maximum resolution up to 0.05 mm. The direction of the wire could also be simply changed by rotating the sensor as shown in enlarged part of Fig. 2. The distance from the inlet of the channel to the wire is 240 mm, which is determined with consideration to the entrance length needed for fully developed laminar flow.

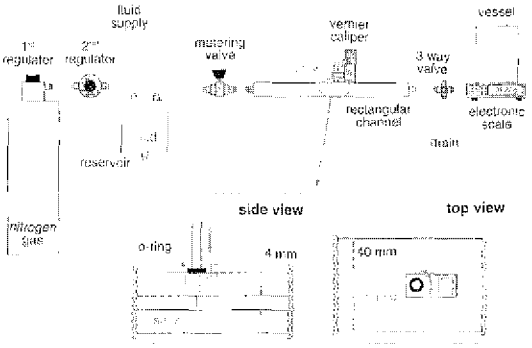

Fig. 2 Schematic of experimental setup

A very stable flow was generated by using pressurized nitrogen gas to push the working fluid in the reservoir into the test section part. The pushed fluid flows into the test section through a metering valve, which precisely controls the flow rate of the working fluid. Ethanol and DI-water were tested as working fluid. The mass of the working fluid which was gathered for a fixed time interval was measured using an electronic scale after the flow was stabilized. The flow rate of the working fluid was calculated from the measured mass of the fluid, the density of the fluid, and the time interval for gathering the working fluid.

In order to obtain the local flow speed at a specific position from the measured flow rate, one should know the relationship between the local

flow speed and the flow rate. The local flow speed of the fully developed laminar flow through a channel of a rectangular cross section is (Panton, 1996)

$$u(y,z)=\frac{1}{\mu}\cdot\frac{dP}{dx}\left[\frac{1}{2}\cdot z(z-c)-2c^2\sum_{n=1}^{\infty}\left(\frac{(-1)^n-1}{(\lambda_n c)^3}\cdot\frac{\sinh\lambda_n y+\sinh\lambda_n(b-y)}{\sinh\lambda_n b}\cdot\sin\lambda_n z\right)\right] \quad (3)$$

where μ is fluid viscosity, dP/dx is the pressure gradient in the streamwise direction of the channel, b and c are the width and the height of the channel as shown in Fig. 3(a), and λ_n is defined as $n\pi/c$. The schematic of the coordinate system is shown in Fig. 3(a). The flow rate obtained by integrating Eq. (3) over the entire cross-section of the channel is

$$Q=\frac{1}{\mu}\cdot\frac{dP}{dx}\left[-\frac{bc^3}{12}-2c^4\sum_{n=1}^{\infty}\left(\frac{((-1)^n-1)^2}{(\lambda_n c)^5}\cdot\frac{1-\cosh\lambda_n b}{\sinh\lambda_n b}\right)\right] \quad (4)$$

The local flow speed at a specific position in the channel can be obtained from Eqs. (3) and (4) using the channel dimensions and the measured flow rate.

The normalized flow speed profiles with the variation of the normal and spanwise direction is shown in Fig 3(b). One can see that the flow speed profile in a normal direction is almost parabolic. On the other hand, the flow speed profile along the spanwise direction is almost flat near the center of the channel.

The phase lag of the sensor temperature with respect to heat generation is measured as follows. When AC current at frequency of ω passes through the sensor, Joule heating induces heat generation at frequency of 2ω in the sensor. Then, the temperature of the sensor oscillates at frequency of 2ω with a phase lag relative to the heat generation. Because the electric resistance of a conductor is a function of its temperature, the resistance of the sensor oscillates with the same

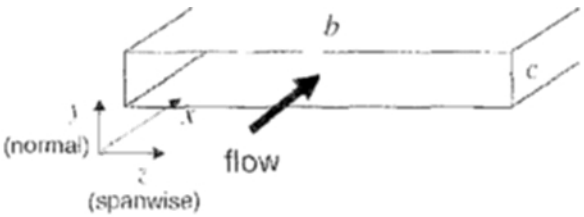

(a)

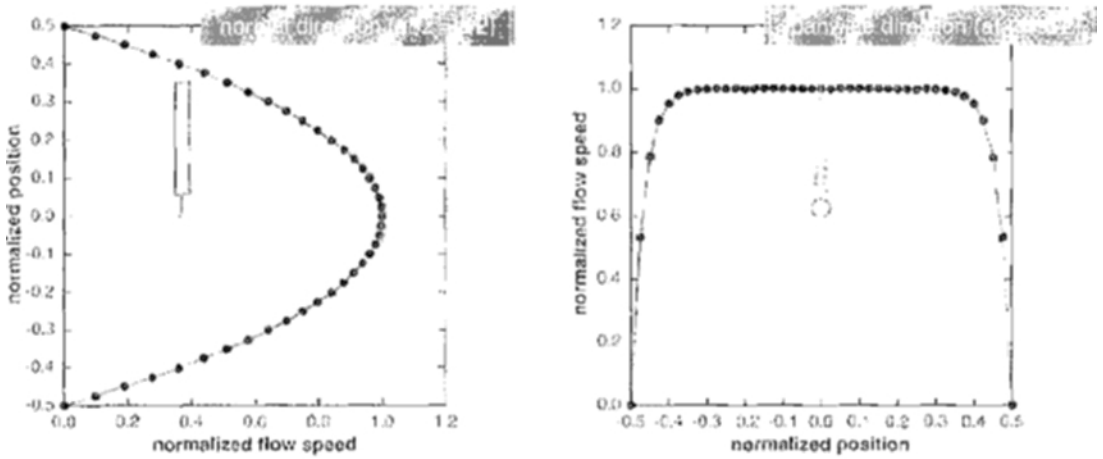

(b)

Fig. 3 Fully developed laminar flow speed profile in a channel of a rectangular cross section (a) Schematic of coordinate system (b) Flow speed profile

frequency and the phase lag as the sensor's temperature. Consequently, because of the original driving current at frequency of ω and the oscillating resistance of the sensor at frequency of 2ω, an AC voltage at frequency of 3ω as Eq. (5) is generated (Chung et al., 2004).

$$V_{3\omega}=\frac{I_0 R_s \alpha T_{s,0}}{2}\sin(3\omega t-\pi+\phi) \tag{5}$$

where I_0 is the amplitude of the driving current, R_s is the resistance of the sensor at room temperature, α is the temperature coefficient of the sensor and $T_{s,0}$ is the amplitude of the sensor temperature oscillation in Eq (2). Hence, one can measure the phase lag from the 3ω voltage signal from the sensor. It is also possible to evaluate the amplitude of the sensor temperature oscillation from the amplitude of the 3ω voltage.

Figure 4 shows a schematic of the circuitry for data acquisition, which consists of a LIA (Lock-In Amplifier), differential amplifiers, an ammeter, an additional resistor and a potentiometer. The circuitry was built with reference to the 3ω method, which is widely adopted for measuring the conductivity of dielectric materials (Cahill, 1990). The phase lag and the amplitude of the 3ω voltage were measured using the LIA, which also has the built-in AC bias for heating the sensor. A potentiometer connected in series with a sensor was used for the purpose of removing the unnecessary ω voltage. Differential amplifiers

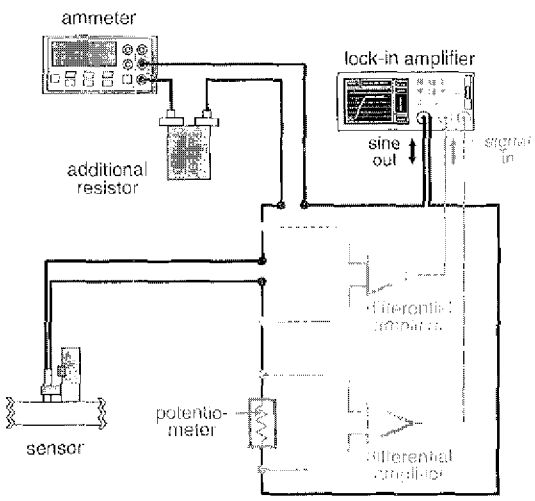

Fig. 4 Circuitry for data acquisition

were used for extracting the voltage signal from the sensor and the potentiometer. For maintaining the current at constant value regardless of the temperature change of the sensor, the additional resistor was used. The current was measured by the ammeter and used for calculating the amplitude of the AC temperature component.

3. Characteristics of Sensor Temperature Oscillation in Stationary Fluid

Because the radius of the sensor is very small and the thermal conductivity of the sensor is much higher than that of the surrounding fluid, the temperature of the sensor can be assumed to be spatially uniform. The temperature of a heated sensor and surrounding fluid at rest can be obtained from the solution of the following equations.

$$\frac{\partial T_f(r,t)}{\partial t}=\alpha_f\left(\frac{\partial^2 T_f(r,t)}{\partial r^2}+\frac{1}{r}\cdot\frac{\partial T_f(r,t)}{\partial r}\right) \tag{6}$$

$$\frac{\partial T_s(t)}{\partial t}=\frac{\dot{q}}{\rho_s c_{p,s}}+2\frac{k_f}{\rho_s c_{p,s} r_s}\cdot\frac{\partial T_f(r,t)}{\partial r}\bigg|_{r=r_s} \tag{7}$$

where T is temperature, α is thermal diffusivity and the subscript s and f represent the sensor and the fluid respectively. Since the heat generation $\dot{q}$ in the sensor varies in a sinusoidal manner, the solutions of Eqs. (6) and (7) can be separated into time and spatially dependent part as follows (Carslaw and Jaeger, 1959)

$$T_f(r,t)=\theta_f(r)\,e^{i(2\omega t)} \tag{8}$$

$$T_s(t)=\theta_s e^{i(2\omega t)} \tag{9}$$

where θ is the complex temperature whose absolute value and argument represent the amplitude and the phase lag of the temperature oscillation respectively. Equation (6) can be transformed into the following equation using Eq. (8)

$$i2\omega\theta_f(r)=\alpha_f\left(\frac{\partial^2\theta_f(r)}{\partial r^2}+\frac{1}{r}\cdot\frac{\partial\theta_f(r)}{\partial r}\right) \tag{10}$$

and the general solution of Eq. (10) is

$$\theta_f(r) = C_1 I_0\left(\frac{r}{d_p}\right) + C_2 K_0\left(\frac{r}{d_p}\right) \tag{11}$$

where I_0 and K_0 are modified Bessel functions of the first kind of order 0 and the second kind respectively. d_p is defined as Eq. (12) and its absolute value $|d_p|$ means the penetration depth of the thermal wave.

$$d_p = \sqrt{\frac{\alpha}{i2\omega}} \tag{12}$$

In Eq. (11), C_1 and C_2 are the constant of integration which are determined by the boundary conditions of the fluid temperature. For satisfying the boundary condition that $\theta_f(r)$ is zero at infinity, C_1 should be zero because I_0 approaches infinity with increasing r. In order to determine the value of C_2, it is necessary to temporarily introduce $\theta_f(r_s)$, which is the complex temperature of the surrounding fluid at the interface between the sensor and the fluid. Also, it is possible to change $\theta_f(r_s)$ into θ_s because $\theta_f(r)$ equals θ_s at the surface of the sensor. As a result, $\theta_f(r)$ is given in the following expression.

$$\theta_f(r) = \theta_s \frac{K_0(r/d_p)}{K_0(r_s/d_p)} \tag{13}$$

Meanwhile, Eq. (7) can be transformed into the following equation using Eq. (9).

$$\rho_s c_{p,s} r_s \cdot i2\omega\theta_s = r_s \dot{q}_0 + 2k_f \left.\frac{\partial\theta_f(r)}{\partial r}\right|_{r=r_s} \tag{14}$$

Combining Eqs. (13) and (14) gives the following equation for the complex temperature of the sensor

$$\theta_s = \frac{r_s \dot{q}_0}{\rho_s c_{p,s} r_s \cdot i2\omega + 2 \cdot \frac{k_f}{d_p} \cdot \frac{K_1(r_s/d_p)}{K_0(r_s/d_p)}} \tag{15}$$

where K_1 are the modified Bessel functions of the second kind of order one.

Figure 5 shows the calculated phase lag of the sensor using Eq. (15). Since the thermal mass of tungsten has a similar value to that of PtRh, there is little difference in the phase lag between the tungsten wire and PtRh wire in the same surrounding fluid (see Fig. 5(a)). However, the thermal conductivity of the surrounding fluid has a significant influence on the phase lag. In the denominator of Eq. (15), the first term is related to the thermal mass of the sensor and the second term to the thermal wave propagation into the surrounding medium. Thermal mass behaves like inertia and causes the phase lag. As the thermal conductivity increases, the influence of the thermal mass reduces and the magnitude of phase lag decreases. Since, the thermal conductivity of DI water is about four times greater than that of ethanol at room temperature, the phase lag of the sensor in DI water is smaller than that in ethanol (see Fig. 5(b)). One can also see that in both

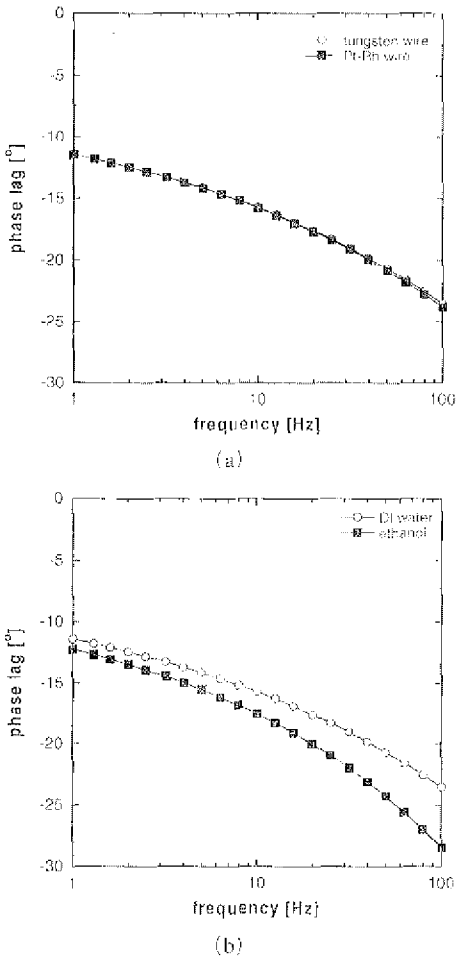

Fig. 5 Phase lag of the wire temperature oscillation (a) from different sensor in Di water (b) from tungsten wire in different surrounding fluid

cases the phase lag becomes larger at higher frequency region because the effect of the thermal mass of the sensor becomes larger at higher frequency region.

Figure 6 shows the comparison between the measured 3ω voltage from experiments and the predicted 3ω voltage using Eqs. (5) and (15) in case of a tungsten wire in DI water ; experimental results matched well with predicted results. In Fig. 6(a), the amplitude of the 3ω voltage is proportional to that of the heat generation (see Eq. (15)). On the other hand, phase lag is nearly independent of the amplitude of the sensor temperature oscillation (see Fig. 6(b)). It's because

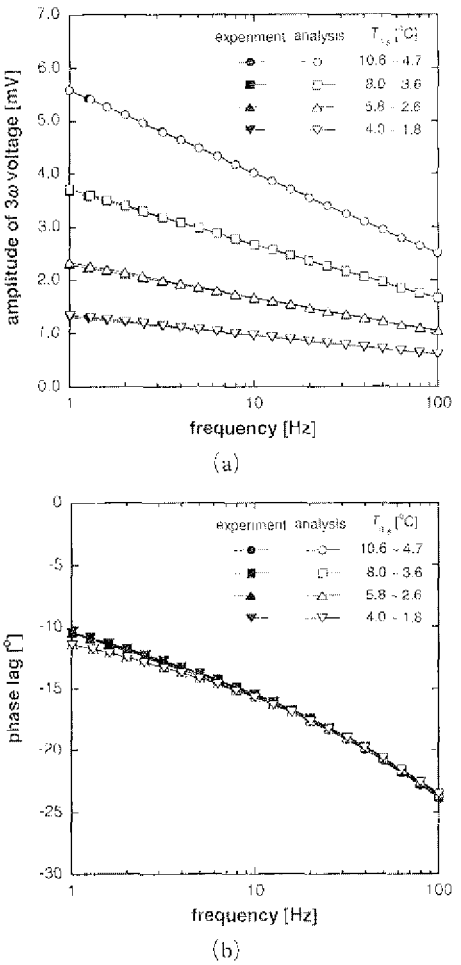

Fig. 6 Comparison of 3ω voltage between experiment and analysis (a) amplitude (b) phase lag (sensor : tungsten wire, fluid : DI water)

the amplitude of the heat generation does not affect the argument of the sensor's complex temperature as shown in Eq. (15).

5. Characteristics of Sensor Temperature Oscillation in Flow Field

In order to find the optimal condition at which the sensor becomes most sensitive to flow speed change, the following experiments were carried out using PtRh wire as the sensor and ethanol as the working fluid. The amplitude and the phase lag of 3ω voltage were measured scanning the heating frequency from 1 to 100 Hz at each fixed flow speed, which was increased from 0.0 to about 50.0 mm/s step by step for each frequency scan. Experiments were conducted at two different amplitudes of temperature ($|\theta_s|=5\sim2$ ℃ and $10\sim4$℃ at rest) in order to make certain that the amplitude of temperature does not affect flow speed measurement. Since the amplitude of temperature varies with frequency even if heat generation is constant, the temperature conditions are given in some ranges. If one wants to keep the amplitude of temperature constant, one may use feedback control and supply power depending on heating frequency. However, one can check the influence of the amplitude of temperature by comparing the measurement results with different amount of heat generation in the sensor.

Dimensionless parameters are used to present the measurement results in more general format. The amplitude of 3ω voltage is presented in dimensionless form defined as

$$V_{3\omega,0}{}^{*}=\frac{V_{3\omega,0}}{\frac{I_0 R_s \alpha |\theta_s|}{2}} \tag{16}$$

where $V_{3\omega,0}$ is the amplitude of the measured 3ω voltage and $|\theta_s|$ is the amplitude of the sensor temperature oscillation in stationary fluid which can be obtained from Eq. (15). This definition of dimensionless 3ω voltage was motivated from Eq. (5). However, the amplitude of the temperature oscillation of the sensor in stationary fluid was used instead of the one in flowing fluid.

Figures 7(a) and (c) show the amplitudes of the dimensionless 3ω voltage for two different amplitudes of temperature, respectively. Comparing Figs. 7(a) and (c), one can see that the amplitudes of the dimensionless 3ω voltage have almost the same value at the same frequency and the same flow speed, independent of the amplitude of heat generation. This shows that the above definition of dimensionless 3ω voltage effectively isolates only the influence of flow speed on the amplitude of temperature oscillation. Figures 7(a) and (c) also show that the amplitude of the dimensionless 3ω voltage is a function of the flow speed and that the amplitude decreases with increasing flow speed at a fixed frequency. The amplitude decreases because the amplitude is inversely proportional to the convective heat transfer coefficient, which increases with the flow speed (see Eq. (1)). This tendency is very obvious in a low frequency region, but the amplitudes at different flow speeds have almost the same value at a high frequency region. This is because the effect of the heat transfer coefficient on the amplitude diminishes with increasing frequency of AC bias (see Eq. (1)).

Figures 7(b) and (d) show the phase lag of the temperature oscillation for two different amplitudes of temperature respectively. One can see that the phase lag of the temperature oscillation has almost the same value at the same frequency

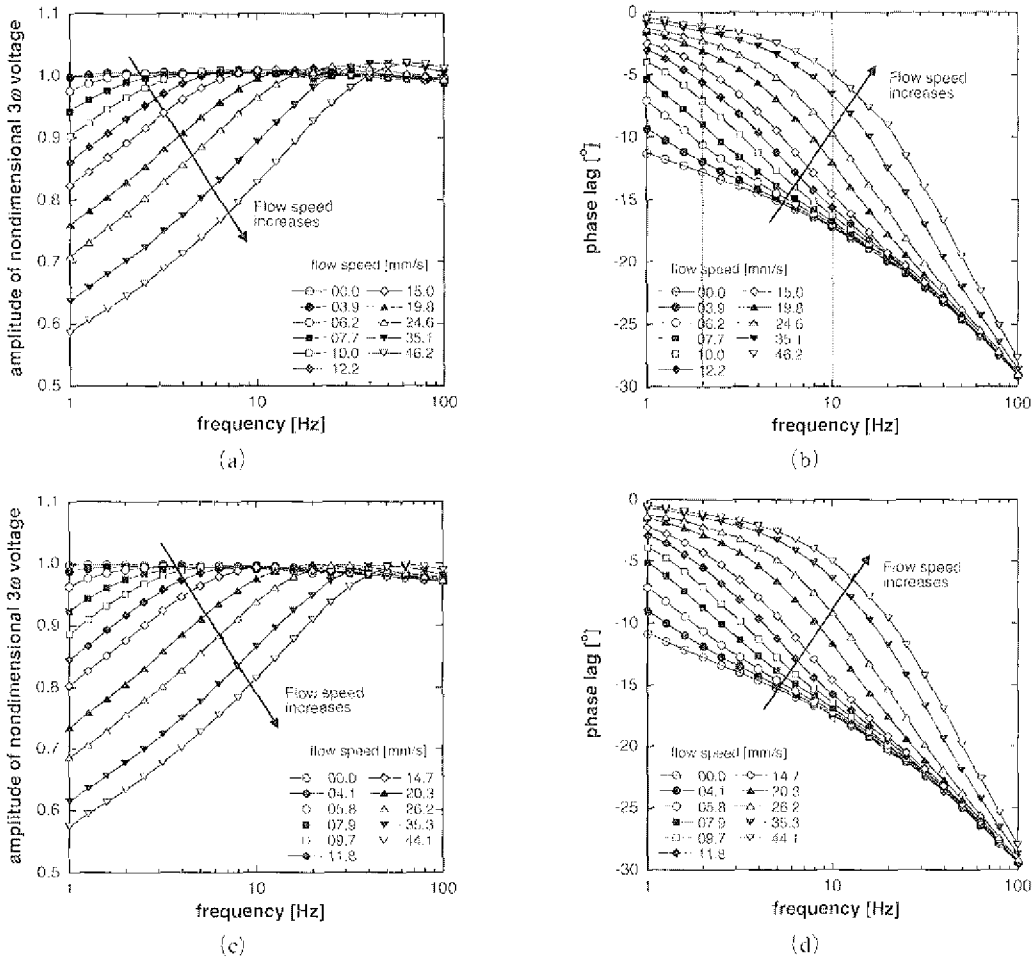

Fig. 7 Measured dimensionless 3ω voltage and phase lag versus frequency for various flow speeds : (a) and (b) for $|\theta_s|=5\sim2$℃ ; (c) and (d) for $|\theta_s|=10\sim4$℃ at rest. (sensor : PtRh wire, fluid : ethanol)

and the same flow speed, independent of the amplitude of heat generation. Quite obviously, this is because this technique measures the phase lag in the frequency domain and the phase lag itself is independent of the heating amount of the sensor. At a fixed frequency the phase lag decreases (approaches zero from negative side) with increasing flow speed. This is because the heat transfer coefficient increases as the flow speed increases (see Eq. (2)). When the flow speed is measured from the phase lag, the measurement sensitivity can be defined by the change of the phase lag with respect to that of the flow speed. Figure 7(b) clearly shows that the optimal condition for the flow speed measurement depends on the frequency of AC bias and the flow speed region itself: the sensitivity for the low flow speed improves in a low frequency region and that for the high flow speed improves in a high frequency region (see the dotted lines in Fig. 7(b)). Therefore, one can measure a very wide range of flow speed by changing the frequency.

Figure 8 shows the difference between the measured phase lag at each flow speed and that at rest as a function of flow speed in various measurement conditions. There is little difference in the measured phase lag difference regardless of the sensor material in Fig. 8(a), as was expected from the result of the phase lag measurement in the fluid at rest (see Fig. 5(a)). However, the phase lag difference is affected by the thermal properties of the surrounding fluid. The phase lag difference measured in ethanol is larger than that measured in DI water at the same flow speed and the same frequency (see Fig. 8(b)). This can be explained as follows. As the thermal conductivity of the surrounding fluid decreases, the influence of convective heat transfer becomes more important than conductive one. Since the convective heat transfer rate is closely related to the flow speed, the sensor becomes more sensitive to flow speed change of fluid with lower thermal conductivity. As mentioned earlier, the thermal conductivity of ethanol is about one fourth of DI water at room temperature. Up until now, all the measurements were carried out keeping the angle between the sensor and the flow 90°. The in-

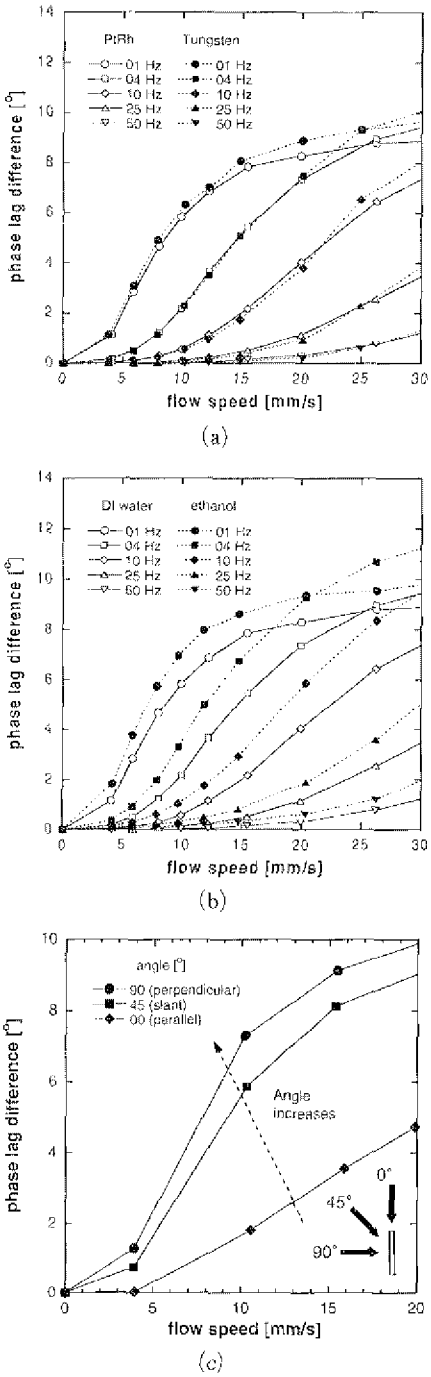

Fig. 8 Results of phase lag measurement (a) using different sensor (PtRh and tungsten wire, fluid: DI water) (b) in different surrounding fluid (fluid: DI water and ethanol, sensor: PtRh wire) (c) at various sensor orientation (angle: 90°, 45°, 0°, sensor: tungsten wire, fluid: DI-water, $f=1$ Hz)

fluence of the angle between the sensor and the flow was tested and is presented in Fig. 8(c). One can see that, at the same flow speed, the phase lag difference increases with the angle between the sensor and the flow (see Fig. 8(c)). It is because the normal component of the flow speed to the sensor increases with the angle. Also, the variation of the phase lag difference is not linearly proportional to that of the angle because the normal component of the flow speed is proportional to the sine function of the angle.

We performed a set of experiments to find the lowest measurable flow speed and the highest resolution, and the results are shown in Fig. 9. The experiments were carried out at 1 Hz of the AC bias frequency because the measurement sensitivity for the low speed flow improves at low frequency region. In order to detect the minute variation of the flow speed, the flow speeds at various vertical positions of a fully developed laminar flow in the channel were measured at intervals of 0.2 mm (see Fig. 9(a)). Only half of the measured data are shown because the parabolic curve formed by the data is symmetric with respect to the center of the channel. The highest resolution measured was 0.05 mm/s near the center of the channel. The data measured at various vertical positions in a fully developed laminar flow were compared with the data measured at the center of the channel with various flow rates (see Fig. 9(b)). A flow speed as low as 1.5 mm/s could be measured. The comparisons of data from different methods of flow speed variation show good consistency, which indirectly validates the experimental facilities and procedures.

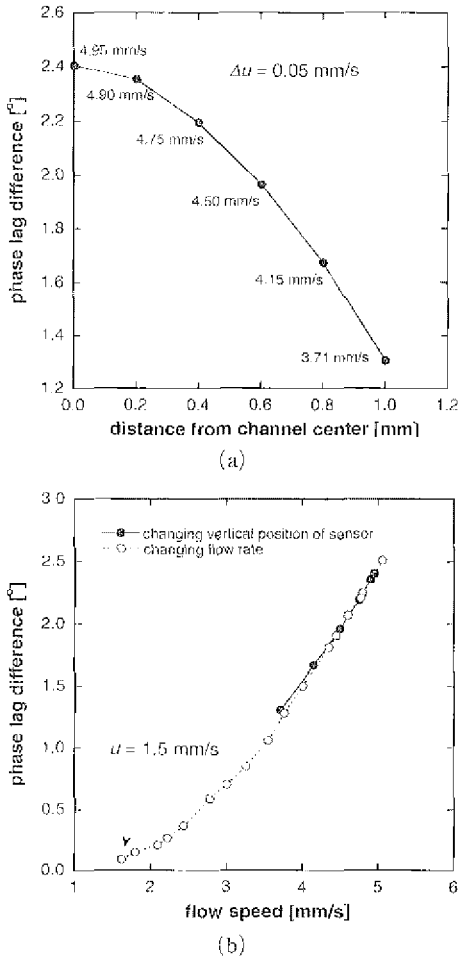

Fig. 9 Results of flow speed measurement (a) changing vertical position of sensor (b) changing flow rate (sensor : PtRh wire, fluid : DI water, $|\theta_s|=10$ ℃ at rest, $f=1$ Hz)

6. Summary and Conclusion

In this paper we experimentally showed the relation between the phase lag and the flow speed to provide the reference data for the effective application of tunable AC thermal anemometry which has several advantages over conventional thermal anemometry.

Before measuring the flow speed, the analytic solution for the sensor temperature oscillation in stationary fluid was obtained in order to verify the measurement accuracy through the comparison with the measurement. The phase lag is influenced by the thermal conductivity of the surrounding fluid. The phase lag in the fluid of higher thermal conductivity is smaller than that in the fluid of lower thermal conductivity. Also, the phase lag becomes larger as the frequency gets higher because the effect of the thermal mass of the sensor, which acts as inertia, increases with the heating frequency. The data from experiment showed good agreement with the analytic solution.

The relation between the phase lag of the 3ω voltage and the flow speed was experimentally investigated at various conditions. The phase lag has almost the same values at the same frequency and the same flow speed and is independent of the sensor temperature. This is because this technique measures the phase lag in the frequency domain. The measurement sensitivity depends on the flow speed and the heating frequency of the sensor. The sensitivity for low flow speed improves in a low frequency region and that for high flow speed improves in a high frequency region. Hence the flow speed in a wide range can be precisely measured by frequency tuning. The measurement sensitivity is also affected by the thermal properties of the surrounding fluid and the sensor orientation. The sensitivity increases with decreasing thermal conductivity of the surrounding fluid because lower thermal conductivity makes the influence of the convective heat transfer more important. The sensitivity decreases with the angle between the sensor and the flow at the same frequency and the same flow speed.

Through performance tests using this experimental setup, the local flow speed could be measured as low as 1.5 mm/s and the highest measurement resolution was 0.05 mm/s in the range of 4.5~5.0 mm/s at 1 Hz. However, if the experiments are carried out with the extremely precise flow control at a lower frequency than 1 Hz, the lower flow speed can be measured with the better resolution.

Acknowledgments

This work was supported by Micro Thermal System Research Center, Seoul National University.

References

Cahill, D. G., 1990, "Thermal Conductivity Measurement from 30 to 750 K : the 3ω Method," *Review of Scientific Instruments*, Vol. 61, No. 2, pp. 802~808.

Carslaw, H. S. and Jaeger, J. C., 1959, "Conduction of Heat in Solids 2nd Edition," *Oxford University Press*.

Chung, W. S., Kwon, O., Choi, D. S., Park, S., Choi, Y. K. and Lee, J. S., 2004, "Tunable AC Thermal Anemometry," *Superlattices and Microstructures*, Vol. 35, pp. 325~338.

Czaplewski, D. A., Ilic, B. R., Zalalutdinov, M., Olbricht, W. L., Zehnder, A. T., Craighead, H. G. and Michalske, T. A., 2004, "A Micromechanical Flow Sensor for Microfluidic Applications," *Journal of Microelectromechanical Systems*, Vol. 13, No. 4, pp. 576~585.

Ernst, H., Jachimowicz, A. and Urban, G. A., 2002, "High Resolution Flow Characterization in Bio-MEMS," *Sensors and Actuators A*, Vol. 100, pp. 54~62.

Oosterbroek, R. E., Lammerink, T. S. J., Berenschot, J. W., Krijnen, G. J. M., Elwenspoek, M. C. and Ben, A., 1999, "A Micromachined Pressure/Flow-Sensor," *Sensors and Actuators*, Vol. 77, pp. 167~177.

Panton, R. L., 1996, "Incompressible Flow 2nd Edition," *John Wiley & Son, Inc.*

Wu, S., Lin, Q., Yuen, Y. and Tai, Y.-C., 2001, "MEMS Flow Sensors for Nano-Fluidic Applications," *Sensors and Actuators A*, Vol. 89, pp. 152~158.

Wu, J. and Sansen, W., 2002, "Electrochemical Time of Flight Flow Sensor," *Sensors and Actuators A*, Vol. 97~98, pp. 68~74.